Solar Energy 135 (2016) 232–241

Contents lists available at ScienceDirect

Solar Energy

journal homepage: www.elsevier.com/locate/solener

High temperature hydrogen production: Design of a 750 KW demonstration plant for a two step thermochemical cycle

J.-P. Säck *, S. Breuer, P. Cotelli, A. Houaijia, M. Lange, M. Wullenkord, C. Spenke, M. Roeb, Chr. Sattler

DLR, Linder Höhe, 51147 Köln, Germany

ARTICLE INFO

Article history:
Received 12 February 2016
Received in revised form 30 May 2016
Accepted 31 May 2016
Available online 8 June 2016

Keywords:
Solar power tower
Thermochemical cycle
Hydrogen
Receiver–reactor
Heat losses

ABSTRACT

The present work describes the study of a solar reactor for a two-step solar thermo-chemical water splitting cycle concerning the EU-project Hydrosol Plant, which aims to build a plant at the end of 2016 on a solar tower at the Plataforma Solar de Almería with a thermal input power of 750 kW to produce 3 kg/week of hydrogen. The process applies nickel-ferrite as reactive species, which works optimally at 1100 °C for the water splitting step and at 1400 °C for the regeneration step. This material is provided in form of monoliths which are used in cars as catalytic converter. On the platform three reactors are placed to reach a volume of about 0.3 m^3 of active material inside the reactor chambers. During the operations two of these will be regenerated while one will work on water splitting, to reach a quasi-continuous hydrogen production. The design concept of the reactor is taken from the SOLREF reactor, which was originally developed by DLR for methane reforming at 900 °C and 10 bar. The scheme and the layout of the plant to feed the reactors have been studied, too. A thermodynamic model for the regeneration step has been also developed to check if the thermal power demand of the three reactors can be supplied by the defined thermal input power. The differences to the other HYDROSOL projects are: The Upscaling from 100 kW to 750 kW, the usage of monoliths completely made of nickel-ferrite and the control strategy with three reactors instead of two.

1. Introduction

The production of hydrogen from water is possible by solar-powered thermo-chemical cycles. A two-step cycle based on a metal oxide redox pair system, which can split water molecules by abstracting oxygen atoms and reversibly incorporating them into its lattice has been developed (Agrafiotis et al., 2005). Several redox materials consisting of oxide pairs of multivalent metals (e.g. Fe_3O_4/FeO (Steinfeld et al., 1999); (Lemort et al., 2006)), Mn_3O_4/MnO (Sturzenegger et al., 1999) or pairs of metal oxide/metal (e.g. ZnO/Zn (Steinfeld, 2002)) have been identified to be able to run the thermochemical cycle in principle. A lot of work has been paid to ferrites doped with a second transition metal (Gokon et al., 2009) and to ceria (Abanades et al., 2006); (Miller, 2007).

The first step is the oxidation of a metal oxide layer by a high temperature steam flow, between 800 °C and 1100 °C: the oxide captures the oxygen in the water, so that hydrogen is released. The oxygen capture is very important because elsewise the separated molecules would spontaneously recombine to water.

$$MO_{red} + H_2O \rightarrow MO_{ox} + H_2 \quad (1.1)$$

The second step is the regeneration of the oxidized metal oxide at temperature between 1100 °C and 1400 °C in an oxygen free atmosphere (N_2): at these conditions the metal oxide releases the captured oxygen and can be oxidized again, closing the cycle (Göhring, 2008).

$$MO_{ox} \rightarrow MO_{red} + \frac{1}{2}O_2 \quad (1.2)$$

The heat power for the reaction could be obtained by the concentration of the solar radiation onto a receiver on a solar power tower plant.

The redox pairs used for this cycle are ferrites and mixed metal oxides with iron as the main component (Allendorf et al., 2006; Kodama et al., 2006; Han et al., 2007). Different approaches on solar receiver concepts for using mixed ferrites have been developed (Kaneko et al., 2006; Allendorf, 2008).

In the HYDROSOL and HYDROSOL-2 project, the metal oxide was coated on SSiC honeycombs, which were placed in the reactor to form a planar surface to absorb the heating radiation (Roeb et al., 2006): the ceramic material can withstand the high temperature of the thermo-chemical cycle but it interferes with the reaction, decreasing the performance of the metal oxide (Neises, 2011).

* Corresponding author.
E-mail address: jan.saeck@dlr.de (J.-P. Säck).

http://dx.doi.org/10.1016/j.solener.2016.05.059
0038-092X/

Nomenclature

A	absorber surface
Ar	area
a	absorptance
CRS	Central Receiver System
c_1	Planck law constant
c_2	Planck law constant
c_p	specific heat at constant pressure
DLR	Deutsches Zentrum für Luft- und Raumfahrt e.V
f	factor
H_2O	water
HYDROSOL	European project
I	insulation layer
i	index
K	correction factor
M	discretized radiation
$\dot{m}$	mass flow rate
MO	metal oxide
Nu	Nusselt number
ox	oxidized
$\dot{Q}$	heat power
$\dot{q}$	heat power flux
p	percentage
Pr	Prandtl number
R	conductive thermal resistance
r_{tot}	Total number of rays
r	radius
Ra	Rayleigh number
red	reduced
Re	Reynolds number
S	sun
SOLREF	SOLar Steam REForming
SSiC	sintered silicon carbide
SSPS	Small Solar Power Systems
T	temperature
U	ambient
W	reactor window
α	convection specific heat exchange coefficient
Δ	step
ε	emissivity
λ	wavelength
λ	thermal conductivity
η	efficiency coefficient
ρ	reflectance
τ	transmittance
φ	view factor

For this project, parallel channels porous monoliths of pure nickel-ferrite, without any substructure, are used to avoid the effect of the ceramic sublayer. This metal oxide has been chosen because the experiments on nickel-ferrite powder has given good results for this kind of thermo-chemical cycle (Agrafiotis et al., 2012) and it has been achieved to manufacture monolith just of this material. The material will now be shaped in foam structure, instead of the honeycomb structure in previous projects. This is, due to the better floating properties of foams regarding the back holding structure, which blocks some outer channels. This avoids hot spots due to convection can take place in every part of the foam. In addition to the previous mentioned advantages of nickel-ferrites, work done within the project proved the good shaping properties of nickel-ferrites into foams, especially the designated, complex shape of the reactor dome, which is analyzed in this paper. In the HYDROSOL 3D project, the reactor and the overall process were pre-designed (Houaijia et al., 2013). Additionally, the overall process including core components, e.g. solar reactors, heat exchangers, compressors, hydrogen separation unit was simulated from a thermodynamic point of view by using the commercial simulation tool Aspen Plus. A detailed exergy analysis was carried out in order to quantify and qualify the exergy losses in the system. The solar receiver–reactor was identified as the pre-dominant source of exergy destruction within the system due the re-radiation losses. An optimized concept of the solar reactor was designed with the support of a raytracing tool. The optimized solar reactor is used in the HYDROSL Plant project und is described in the next chapter.

The differences to the other HYDROSOL projects are: The Upscaling from 100 kW to 750 kW on a solar tower system, the usage of monoliths completely made of nickel-ferrite to solve the problems with the coating on ceramic structures and the new control strategy with three reactors instead of two relating to the slow kinetics of the regeneration process.

2. Reactor concept design

The reactor has to stand temperature up to 1400 °C while it works at ambient pressure. The design concept is taken from other reactor developments by DLR in the past to reform methane at 900 °C and 10 bar, so called SOLREF (Möller et al., 2006) and air heating, so called REFOS (Buck et al., 2002) (see Figs. 1, 5 and 6).

The reactor has a maximal diameter of 1100 mm and a length of about 1500 mm without secondary concentrator and a length of about 2450 mm with secondary concentrator and consist of 5 main components (Fig. 2).

The secondary concentrator protects the frontal flange from the direct radiation coming from the heliostats, to use this spillage in the reactor instead of losing it, and to homogenize the solar radiation as much as possible hitting the receiver window. It has a dodecagon shape made by twelve trapezoidal metal sheets to form a kind of Compound Parabolic Concentrator (CPC): the diameter of the inscribed circumference of the dodecagon shape outlet is 560 mm diameter and it is connected to the front flange with three M14 screws.

The window has a dome shape with a diameter of 652 mm, a length of 450 mm and a thickness of 8 mm: it is assembled on a sealing ring, which is hold by a small flange screwed to the front

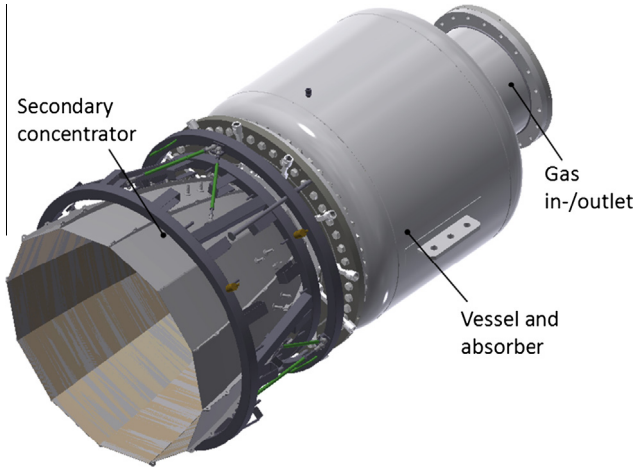

Fig. 1. View of the Hydrosol reactor.

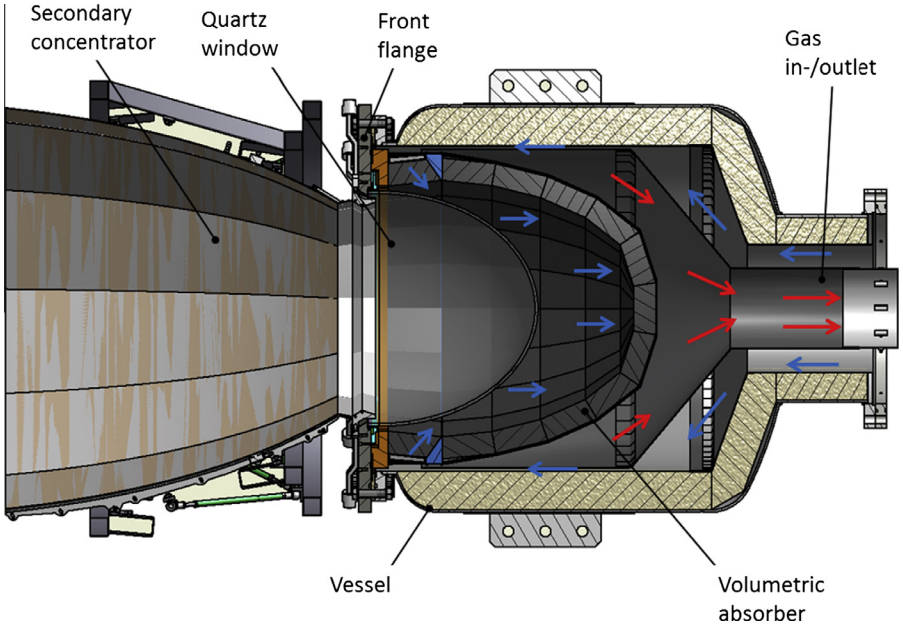

Fig. 2. Hydrosol reactor design concept.

flange inside the reactor and cooled by a nitrogen stream coming through it (Fig. 3). The sealing effect is ensured by the pressure inside the reactor that pushes the window against a sealing ring placed on the front flange: this system has been developed by DLR for systems with overpressure of at least 1 bar inside the reaction chamber. The overpressure will be very low, less than 0.5 bar, just to make the stream overcome the pressure drop in the system, thus, the former sealing won't work perfectly, allowing some educt gases to leave the reactor. This shouldn't be a problem for the operation because it is just important for the process that no air can flow inside the reactor, because the redox material would absorb easier the oxygen from the air than from the water and this is avoided by the slightly overpressure of the incoming stream.

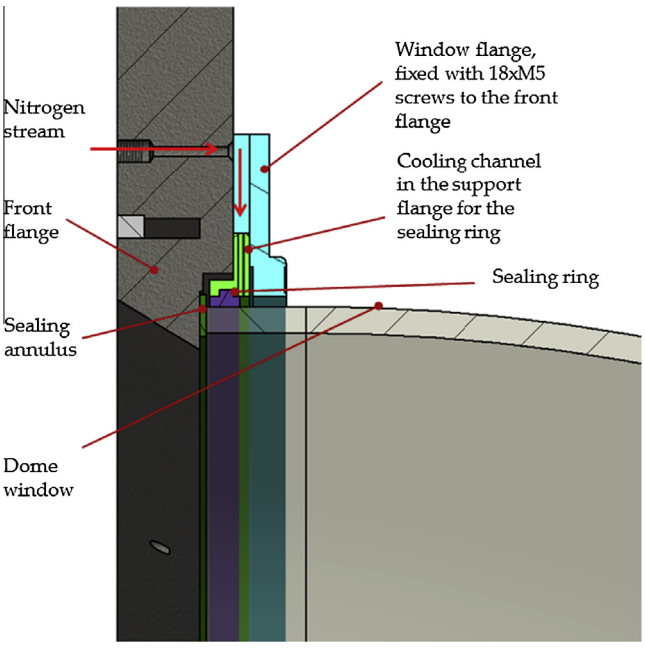

Fig. 3. Detailed section of the dome window mounted on the front flange.

The front flange of the reactor is an annular plate with an inside diameter of 615 mm and an outside diameter of 1100 mm and a thickness of 35 mm. It has to fix the secondary concentrator and the window. On the flange, three cooling systems are placed to cool the flange itself, the quartz window and the silicon ring holding the window. The flange is cooled by a refrigerant mixture consisting of demineralized water and an antifreezing compound flowing through two concentric channels placed at diameters of 677 mm and 864 mm and with a rectangular section of 6×12 mm^2. The window cooling system is adapted from the SOLREF and REFOS reactors and is composed by twelve extensions screwed on the front side, which hold twelve ducts with a rectangular section in which compressed air can flow along the dome window: the ducts are fed one by one to avoid a hot spot at the top of the window and to create a vortex, which increases the turbulence of the cooling stream and thus the heat exchange. These extensions are also important because they shield the components at the front from the direct solar radiation: because of this, the bottom surfaces are coated with backsilvered mirrors and are cooled by a water cooling channel. The third cooling system is a nitrogen stream, which is fed into six circumference holes to cool the sealing ring. The flange is connected to the vessel by fifty M20 screws, so that it can be disassembled to make some maintenance work on it or to extract the absorber structure.

The absorber structure has an elliptical shape to reduce the losses of the radiation emitted from the absorber to the environment: it has a tilted inlet ring and a concave outlet region formed by five parallel rings and one central element. Each ring is formed by 18 parallel channels porous monoliths cut to form a roman arc structure, so that the monoliths cannot fall down into the cavity once assembled: the total volume of active material in a cavity is 95 l (Fig. 4). The holding structure for the cavity will be developed by a German company and will be made of a high temperature ceramic fiber composite material based on alumina. The holding structure is only located at the backside of the absorber dome. Behind the outlet absorber, the outlet flow is split from the inlet one by an inner case: this will be constructed with the absorber holding structure because no steel can withstand temperature of about 1400 °C. A middle case separates the inlet flow from the thick insulation layer between this and the external one. On the

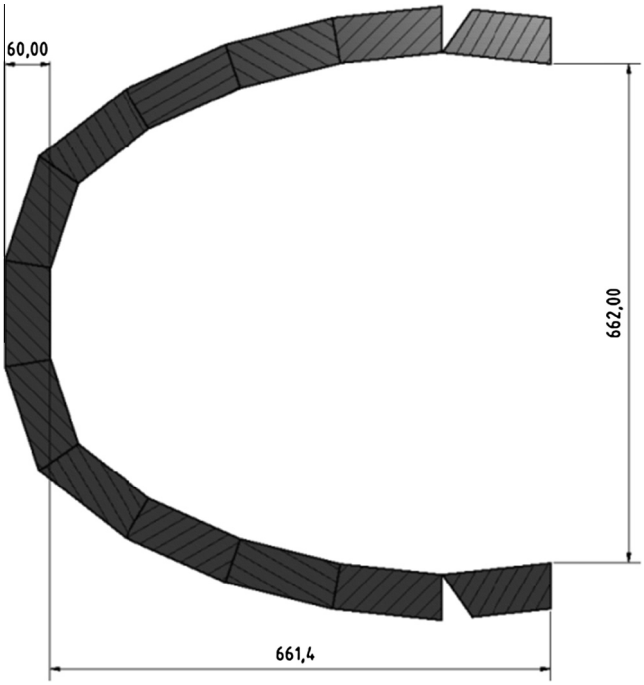

Fig. 4. Volumetric absorber shape.

front and on the back of the reactor two flanges are mounted in which it is possible to place temperature and pressure sensors to control properly the temperature of the absorber and of the inlet and outlet streams.

The flow is launched in the reactor between the inner and outer case. It flows through the inlet absorber and is heated up by the outlet flow, which flows inside the inner case. The flow comes in the reaction chamber where it is heated up until the reaction temperature by the radiation of the sun hitting the absorber surface: when the flow gets in contact with the absorber at the reaction temperature, the production of hydrogen during the splitting or releasing oxygen during the regeneration step takes place. After this, the stream or nitrogen flows across the absorber until the outlet pipe, where some heat recovery takes place.

For improving the overall plant efficiency in temperature based processes, a good heat management has to be pursued. Therefore, a simplified heat recovery system has been developed, based on two heat exchanger; one for each of the hydrogen and nitrogen path. In this case, the heat exchanger are not controlled, but rather used as pre-heaters. This allows, getting a good look at the usage of heat exchanger type and materials for the applied high temperatures (up to 1400 °C). Considering heat losses after the gases leaving the reactor, the heat exchanger are built for temperatures up to 1100 °C, so non-iron metals or high alloyed steels, like nickel based alloys, can be used. For safety reasons, the maximal allowed temperature, of the gases, is set to 800 °C. While the experimental campaign is running, the inlet gas temperature will be raised subsequently to 1100 °C. The preheating is calculated to the following values (based on the 800 °C):

Inlet (to reactor)	Outlet (from reactor)
H_2O: 120–716 °C	H_2O: 800–218 °C
N_2: 150–662 °C	N_2: 800–300 °C

Those values can be understand as a good estimation, but they will be validated during the experimental campaign.

3. Plant design

The mass flow rates are 10 kg/h for the steam and 200 kg/h for the nitrogen: these have been chosen in according with the developer of the redox material and budget reasons. The plant is placed on two floors on the Small Solar Power System (SSPS-CRS) solar tower at the Plataforma Solar de Almería: the floor for the reactors is placed at 26 m high and it has a surface of about 6×4 m^2; the second one is just under this floor where the peripheral components will be placed. During the operation, two reactors will be regenerated, while one will produce hydrogen. This is based on the slower kinetics during regeneration.

The water flows inside an electrical evaporator and then into a heat exchanger, which recovers the heat of the stream coming out of the reactor on water splitting. After that, the steam is driven into the reactor which has to produce hydrogen: at the outlet, the flow composition is analyzed by a mass spectrometer. Afterwards, the product stream flows into the heat exchanger and then in a condenser, which separates the not reacted steam from the produced hydrogen. The nitrogen stream flows inside an heat exchanger, which recovers the heat from the nitrogen coming out of the reactor, and then flows into the reactors to regenerate. The out coming flows of the reactors are exhausted into the atmosphere after the heat exchanger because the nitrogen will contain some oxygen and cannot be used again in the plant. The flows at the inlet and outlet of each reactor are controlled by butterfly valves. For bigger plants it is thought of regenerating the nitrogen flow. This is important for efficiency reasons, due to the high amount of needed N2. A promising possibility of regenerating N2 is to use another thermochemical cycle for air separation. Ezbiri showed the usability of perovskites in $SrCoO_3$ composition. The temperature cycle was executed with 900 K for the reduction and 600 K for the oxidization. This perovskite outperforms the state-of-the-art copper cycle. Furthermore, the copper cycle cannot be used with this lowgrade process heat of 600–900 K (Ezbiri et al., 2015). Nevertheless, for this demonstration plant, technical available N2 will be used.

The reactors are placed on the floor to form a triangle, with two on the floor and one hanging from the roof and are 14° tilted in respect to the horizontal direction to point the center of the heliostats field. The form of a triangle was chosen because of the usage of spillage of each reactor for the other ones. This is based on the good results in the Refos project (Buck et al., 2002). The two heat exchangers are placed on the same floor to reduce the heat losses in the plant and to reduce the length of the pipes at high temperature, while the other components of the plant are placed downstairs.

4. The thermodynamic model of the reactor

The valuation of the heat losses in the reactor is important to know if there is enough power for heating the absorber surface and the gas flow to the working conditions. Since, the reactor already existed and thus adapted for the new use of thermoschemical water splitting, the thermodynamic model had to be adjusted to the actual reactor design. The following simplified model was created to run the calculations.

The reactor is evaluated as a hemisphere, where the flat surface is the quartz window and the curved one is the absorber, in that way it is easier to study the radiation phenomena, imposing a uniform distribution of radiation on it. The hemisphere is sized so that the absorber surface and the view factor correspond to the real absorber shape extension. The space between the absorber and the window is supposed to be perfectly insulated to simplify the model. The variables are the window temperature, T_W, and the absorber temperature, T_A, both evaluated as a constant temperature body.

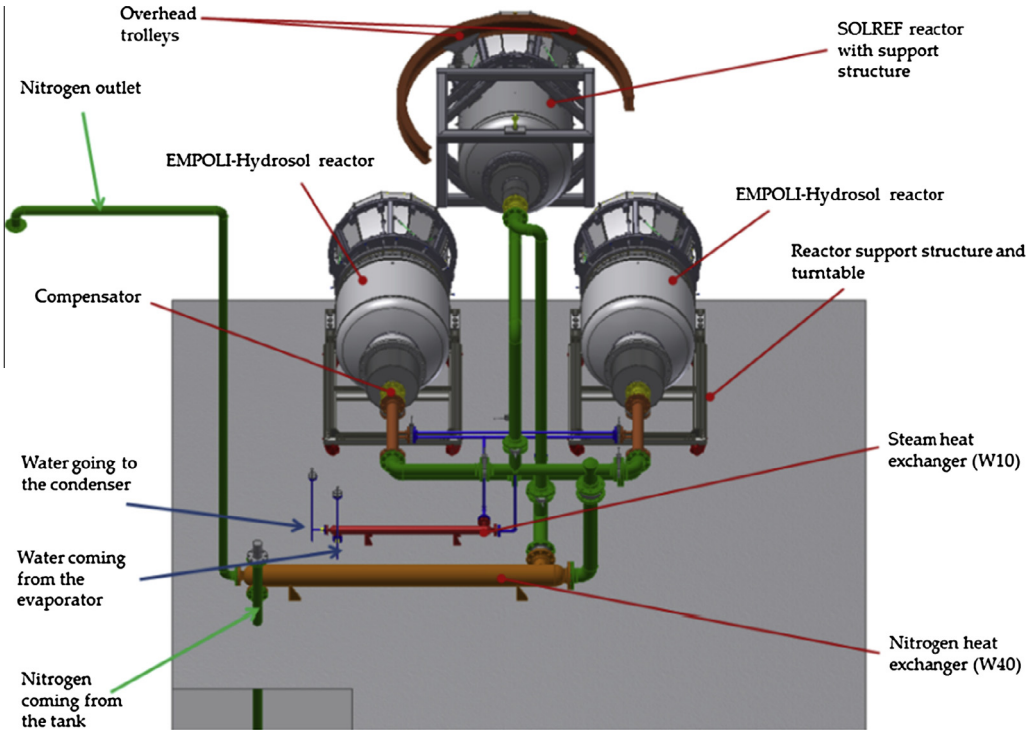

Fig. 5. Plant layout from the back side.

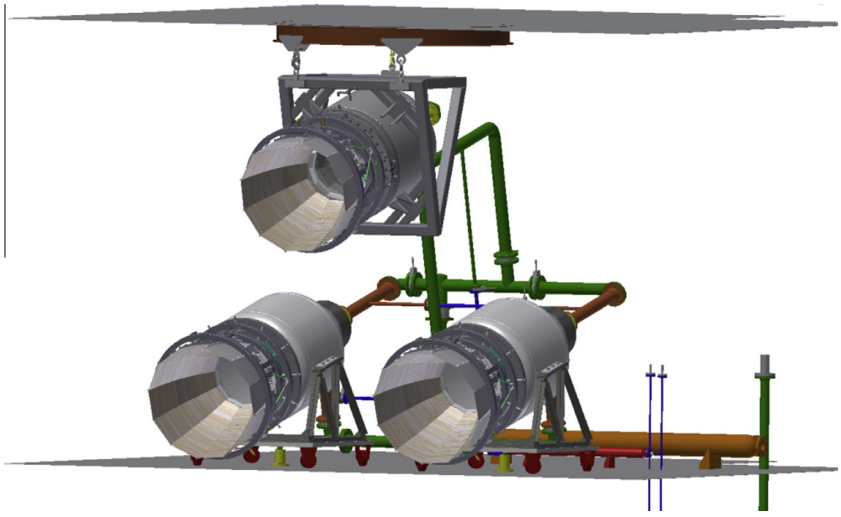

Fig. 6. Plant layout from the front side.

The optical properties of the quartz window have a big dependence on the incidence angle and wavelength of the incoming radiation and on the glass temperature. Because of this, it is important to estimate the distribution of the incidence angle of the radiation on the window to get a more realistic calculation. This is not easy to get because the solar radiation doesn't hit directly the window, it comes from the heliostats and passes first through the secondary concentrator. A ray–tracing software, called OPTICAD®, is used to estimate how the radiation is hitting the window (Opticad-Corporation®, 2008).

Because the heliostats field is symmetric, just one half and the central line are added to the model as ideal parabolic mirrors of the dimension of the used Martin Marietta heliostats at the PSA ($6.4 \times 6.4\ m^2$), so that it is easy to focus them on the reactor window. The position of the heliostats is shown in Fig. 7, where the yellow numbers are the heliostats of the field planned to be used in the project: in total they are 59. In Fig. 8 the half heliostats field modeled in OPTICAD® is shown.

Then, the secondary concentrator is added by importing the cad model of the real component. This is placed in the middle position of the three reactors on the platform: along the central line of the heliostats field, at the tower distance and at 26.5 m high. Finally, a flat receiving surface is added at the end of the concentrator, so that the incidence angle of all rays can be detected and saved by the software.

The sun is placed on the south direction with a solar altitude angle of 45°. As simplification, the solar rays are supposed to be parallel. To make the focusing of each heliostat easier, a light

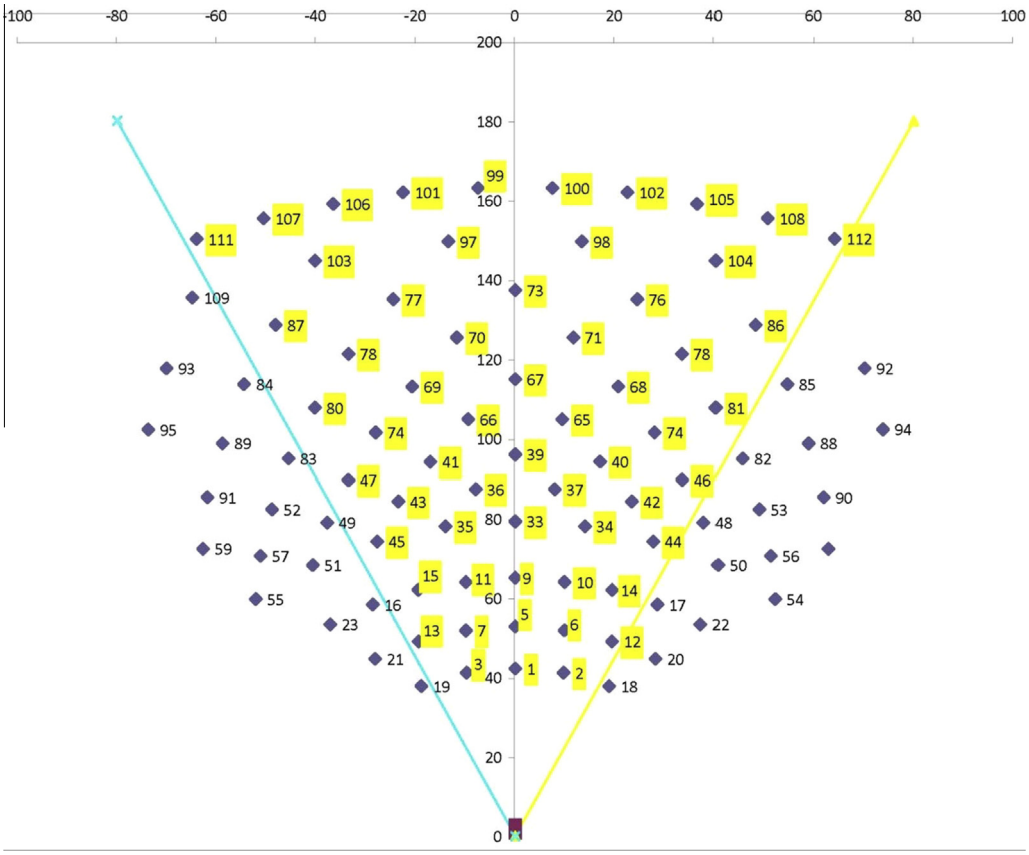

Fig. 7. Complete heliostats field at the PSA.

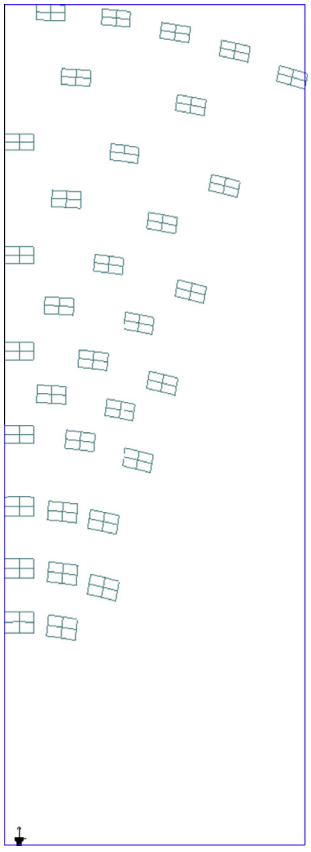

Fig. 8. OPTICAD® model of the heliostats field.

source is created for each one and the data of the receiving surface is collected as well. Each light source emits parallel rays on the heliostats surface which are reflected to the secondary concentrator.

Once the data for each heliostat is collected in one excel file, this data has to be used to get a distribution of the incidence angle. The secondary concentrators have got an aperture angle 40°. In case of this only heliostats inside this aperture angle where chosen (see Fig. 7). It is noticed that the 98.5% of the rays have an incidence angle smaller than 40° and the optical coefficients doesn't change strongly with the incidence angle before of that: the distribution can be so studied with a rather large discrete intervals. The rays are collected in 18 groups with an interval of 5° from 0° to 90°. Once the rays are collected in these groups, the discrete distribution is easily calculated by dividing the total number of the rays in each group i, $r_{tot,i}$, to the total number of the rays hitting the window, r_{tot}.

$$p_i = \frac{r_{tot,i}}{r_{tot}} \quad i = 1 \ldots 18 \tag{4.1}$$

$$r_{tot} = \sum_{j=1}^{18} r_{tot,i} \tag{4.2}$$

Because in the software just the right half of the heliostats field is implemented, the rays of the missing part are extrapolated from the symmetric part of the field.

The resulting distribution is shown in Fig. 9. It can be noticed that almost all of the radiation hits the window between 0° and 40° and almost 30% of the radiation comes on the window with an incidence angle between 15° and 20°. Just a very small part of the radiation comes with bigger angles, that means that the heliostats field is

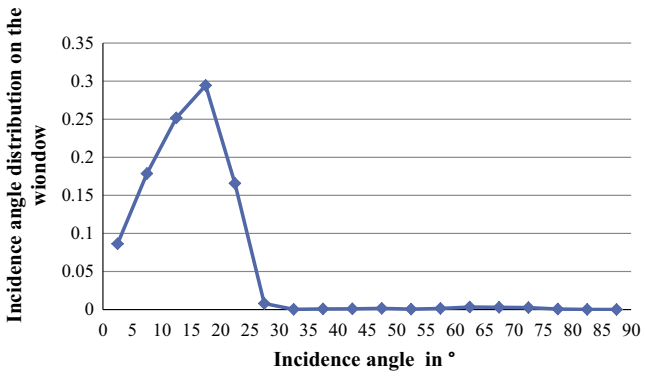

Fig. 9. Incidence angle distribution for the entire heliostats field.

small enough to focus on the window almost perfectly; just some rays coming from the heliostats at the border or at the bottom hits the surface of the concentrator and mostly very close to the window: these rays come with an very big angle between 60° and 70°. Actually, the real mirrors will have a worse behavior, due to the optical and geometrical losses and because they are Fresnel mirrors and not parabolic ones, but an accurate analysis of the field is not the purpose of this simplified model for the plant. About the incidence angle distribution, it will be assumed that no radiation hits the window with an incidence angle bigger than 40° to run faster the calculation. During the project it is planned to measure the real mirror surface of the heliostat mirrors with deflectometry for further simulations with ray tracing software.

The thermodynamic model has been developed considering four parts: the ambient, the window, the absorber and the insulation, named respectively as U, W, A and I in the following formulas. Each of this parts exchanges heat through conduction, convection and radiation phenomena, which are described and modeled in the following part of this section (Fig. 10).

On the outside of the window, the heat exchange takes place in four different ways: the radiation from the heliostat field, the emission of the window, a natural convection cooling with the ambient air and a forced cooling due to the cooling system on the window. The solar radiation has to be calculated: the radiation power coming from the heliostats is $\dot{Q}_{S,W,rad}$ during the regeneration step and a spillage loss of 20% is taken into account, because the annual efficiency of the field is about 90% in comparison with the design point and there are other losses due to the not perfect focus of the far heliostats into the reactor opening.

The window is evaluated as a flat disc of 621 mm diameter and the flux density on that is just the ratio between the solar power and the surface, as shown at the Eq. (4.3), where η is the spillage loss.

$$\dot{q}_{S,W,rad} = \frac{\dot{Q}_{S,W,rad} \cdot (1-\eta)}{A_w} \tag{4.3}$$

The total solar radiation $M_{tot,S}$ and the solar radiation per wavelength $M_{\lambda,S}$ are calculated with the discretized Planck law (Martin, 2006): the wavelengths are discretized with a 0.01 μm step. About the solar radiation, the ratio f between $M_{tot,S}$ and $\dot{q}_{Hydr,W,rad}$ is a factor to distribute the power coming from the heliostats to the window on the radiation wavelength: in this way, it is possible to calculate the energy absorbed, transmitted and reflected for each discretized wavelength.

$$f = \frac{M_{tot,S}}{\dot{q}_{S,rad,W}} \tag{4.4}$$

$$\dot{q}_{\lambda,S,W} = M_{\lambda,S} \cdot f \tag{4.5}$$

$$\dot{q}_{\lambda,S,W,\rho} = q_{\lambda,S,W} \cdot \rho_\lambda \; \dot{q}_{\lambda,S,W,t} = q_{\lambda,S,W} \cdot \tau_\lambda \; \dot{q}_{\lambda,S,W,a} = q_{\lambda,S,W} \cdot a_\lambda \tag{4.6}$$

$$\dot{q}_{\lambda,S,W} = \dot{q}_{\lambda,S,W,\rho} + \dot{q}_{\lambda,S,W,t} + \dot{q}_{\lambda,S,W,a} \tag{4.7}$$

The calculation of the optical factors ρ_λ, τ_λ and a_λ is not easy because they depend on the ray incidence angle and on the temperature of the quartz window: a table with the optical factors values for wavelengths from 0.250 μm to 80 μm with step of 0.01 μm, incidence angles from 0° to 90° and at temperature of 25 °C and 700 °C was studied in DLR during a test campaign and it has been used to evaluate the coefficients in the model. The different incidence angles are grouped in 18 steps of 5° and the reference optical coefficients for each step are the coefficients of the angle at the centre of each interval. These coefficients have been weighted than using the distribution of the incidence angle on the flat window carried out from the ray-tracing simulation.

The optical factors ρ_λ, τ_λ and a_λ are calculated for the two available temperature, 25 °C and 700 °C. Finally, a linear interpolation is done also between the two temperatures, so that the factors can be calculated for every temperature we have, supposing a linear behavior of the material.

$$\dot{Q}_{S,rad,W,i} = \Delta\lambda \cdot \sum_{\lambda=0.25}^{\lambda=80} q_{\lambda,S,W} \cdot i_\lambda \quad i = \rho, a, \tau \tag{4.8}$$

The exchanged heat from natural convection on the window with the external ambience (Eq. (4.9)) is calculated with the heat transfer coefficient evaluated by the natural convection Nusselt number formula for a flat surface and with ideal gas (Eqs. (4.10) and (4.11)), valid for Rayleigh number between 10^{-1} and 10^{12}: in this case, the calculated Rayleigh number is about $2.5 \cdot 10^8$. This result ensures the correctness of the used formula for calculating the heat exchange values. The properties of the air are calculated by using the temperature dependent equations of the physical properties, which are polynomials extrapolated from the tabulated values, at the middle temperature between the ambient and the window temperature (Martin, 2006).

$$\dot{Q}_{W,conv,U} = \alpha_{W,conv,U} \cdot A_W \cdot (T_W - T_U) \tag{4.9}$$

$$f_1 = \left[1 + (0.492/Pr)^{9/16}\right]^{-16/9} \tag{4.10}$$

$$Nu_{W,conv,U} = \left(0.825 + 0.387[Raf_1(Pr)]^{1/6}\right)^2 \tag{4.11}$$

The cooling system on the window is just modeled as a power loss on the window $\dot{Q}_{W,fcooling}$, which can be set as the user wants: this simplifies the effect of the cooling on the window and gives an idea of the needed cooling power to stay under a critical temperature for the system.

The window emits a considerable amount of energy because of its temperature: this radiation is calculated for a grey body with the emissivity equal to the absorptivity for each wavelength ($\varepsilon_\lambda = a_\lambda$). Because the emitted radiation is homogenous to the entire environment, the emissivity coefficient is calculated from the absorption coefficient considering a uniform emission to all the directions.

The radiation power is calculated by the Planck law. The window irradiates because of its flat shape half into the reactor and half outside.

$$\dot{Q}_{W,rad,U} = \dot{Q}_{W,rad,A} = \Delta\lambda \cdot \sum_{\lambda=0.25}^{\lambda=80} M_{\lambda,W} \cdot \varepsilon_\lambda \tag{4.12}$$

$$M_{\lambda,W} = \frac{c_1}{\lambda^5 \cdot (e^{c_2 T_W} - 1)} \tag{4.13}$$

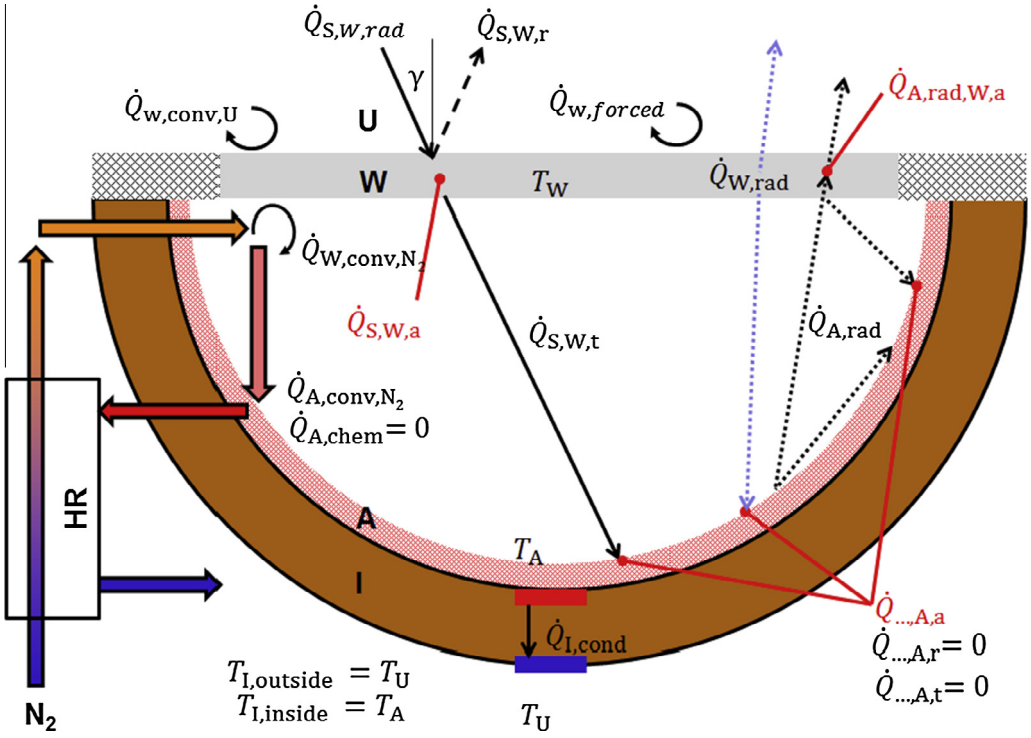

Fig. 10. Scheme of the reactor thermodynamic model.

The absorber is defined as a black body: this means that it can only absorb and emit radiation, but not reflect or transmit any radiation. This assumption has two main reasons: the first is that an eventual reflection of the absorber surface would make the model more difficult because the reflected radiation would be partly reflected back from the window generating a bouncing effect between the inner reactor surfaces. Then, the absorber material has an absorptivity of round about 0.9 in according with its developer and it is shaped in honeycombs, which generate light diffusion phenomena on the radiation, which doesn't hit a compact surface, decreasing the reflection coefficient of the material. The absorber surface in the model is taken equal to the real absorber surface, which is calculated with the CAD software to be 1.36 m^2. Because it has a certain temperature, also this body emits radiation following the Planck law with an emissivity of 1, assuming black body behavior as for the sun. The radiation in part hits the windows and in parts the absorber: the cavity geometry of the model allows us to use simple view factor equations, shown in Eq. (4.14) (Martin, 2006).

$$\varphi_{WA} = 1 \quad \varphi_{AW} = A_2 \cdot \frac{\varphi_{21}}{A_1} = 0.78 \quad \varphi_{AA} = 1 - \varphi_{12} = 0.22 \tag{4.14}$$

From this calculation it results that about eighty percent of the absorber radiation hits the absorber, while the other part hits the window, where it can be reflected, transmitted or absorbed: the optical coefficients of the quartz window are calculated in the same way as for the emissivity because the radiation coming from the absorber can be assumed uniform since each point radiates to all the directions.

$$\dot{Q}_{A,rad,A-W} = \dot{Q}_{A,rad,A-A} = \varphi_{AW} \cdot \Delta\lambda \cdot \sum_{\lambda=0.25}^{\lambda=80} M_{\lambda,A} \tag{4.15}$$

$$\dot{Q}_{A,rad,A-W,i} = 0.5 \cdot \Delta\lambda \cdot \sum_{\lambda=0.25}^{\lambda=80} M_{\lambda,A} \cdot i_\lambda \quad i = \rho, a, \tau \tag{4.16}$$

The absorber than has also a conductive heat transfer with the ambient through an insulation layer: the calculation is done for concentric spherical surfaces. The insulation thermal resistance is shown in Eq. (4.17) (Martin, 2006). The external temperature is assumed to be equal to the ambient temperature. The thermal conductivity λ is set to 0.5 W/m K, because it is a typical value for the alumina based insulation, which will be placed in the reactor (Morgan®, 2013).

$$R_{I,cond} = \frac{r_2 - r_1}{2\pi\lambda r_1 r_2} \tag{4.17}$$

$$\dot{Q}_{I,cond} = \frac{T_A - T_U}{R_{I,cond}} \tag{4.18}$$

The last heat contribution in the model is the working flow, which has to be heated up from the inlet temperature in the reactor to the reaction temperature. Because the regeneration step is the one at higher temperature and with higher mass flow, this is taken into consideration for the calculation in the model. The nitrogen mass flow is set to 100 kg/h, which is the maximal planned quantity per reactor for the plant. The heating is divided in three phases: the heat recovery, in which the out-coming flow heats up the incoming flow, the convection with the window and, finally, with the absorber; the power for the chemical reaction to release the oxygen from the redox material can be neglected because it is very small in comparison with the other heat fluxes because of the very few amount of oxygen absorbed and released by the redox material. At the end, the temperature of the nitrogen is imposed to be equal with the temperature of the absorber. The heat recovery part is simply given as a percentage: the outlet gas heats up the incoming flow at ambient temperature, by exchanging with it a certain percentage p_{HR} of the needed energy to be heated up to the absorber temperature. The value is assumed so that the temperature of the nitrogen at the inlet is round about 650 °C, which

is the expected outlet temperature of the nitrogen from the heat recovery part of the plant. From this equation, the temperature at which the stream flows inside the reaction chamber is calculated.

$$\dot{Q}_{N2,heatrecovery} = p_{HR} \cdot \dot{m}_{N2} \cdot \overline{c_p}_{N2,A-U} \cdot (T_A - T_U) \tag{4.19}$$

$$T_{N2,In} = T_U + \frac{\dot{Q}_{N2,heatrecovery}}{\dot{m}_{N2} \cdot \overline{c_p}_{N2,U-In}} \tag{4.20}$$

The convection with the window is modeled as a superimposed forced and free one because the stream speed, estimated as the ratio of the reactor inlet volume flow rate at the temperature $T_{N2,In}$ with the window surface A_W, is low, less than 0.5 m/s, and the natural convection cannot be neglected. The Nusselt number formula for the forced convection is calculated from the equation for a laminar flow on a planar surface at uniform temperature, with a correction factor due to the direction of the heat flux (Eqs. (4.21) and (4.22)). The Nusselt number formula for the free convection is taken for a vertical planar surface as for the outside of the window (Eqs. (4.9) and (4.10)). The total Nusselt number is a combination of the two calculated equations (Eq. (4.23)). All the properties of the nitrogen streams are calculated at the average temperature between the two surfaces, on which the exchange takes place, by using the temperature dependence equations as for the air (Martin, 2006).

$$Nu_{W,conv,N2\_forced} = K \cdot 0.664 \sqrt{Re_l} \sqrt[3]{Pr} \tag{4.21}$$

$$K = \left(\frac{\overline{T}_{N2,In-W}}{T_W} \right)^{0.12} \tag{4.22}$$

$$Nu_{W,conv,N2} = \left(Nu^3_{W\_free} + Nu^3_{W\_forced} \right)^{1/3} \tag{4.23}$$

$$\dot{Q}_{W,conv,N2} = \alpha_{W,conv,N2} \cdot A_W \cdot (T_W - \overline{T}_{N2,In-W}) \tag{4.24}$$

$$T_{N2,W} = T_{N2,In} + \frac{\dot{Q}_{W,conv,N2}}{\dot{m}_{N2} \cdot \overline{c_p}_{N2,In-W}} \tag{4.25}$$

From the Nusselt number, the heat transfer coefficient and the exchanged heat can be calculated with Eq. (4.24). Eq. (4.25) gives an average temperature for the stream in the first part of the reactor. The necessary heat to warm up the stream to the absorber temperature can be easily calculated with Eq. (4.26).

$$\dot{Q}_{A,conv,N2} = \dot{m}_{N2} \cdot \overline{c_p}_{N2,W-A} \cdot (T_A - T_{N2,W}) \tag{4.26}$$

The outlet temperature is then evaluated with Eq. (4.28), so that the flow heats up the inlet stream up to the defined temperature in the reaction chamber.

$$T_{N2,Out} = T_A - \frac{\dot{Q}_{N2,heatrecovery}}{\dot{m}_{N2} \cdot \overline{c_p}_{N2,A-Out}} \tag{4.27}$$

Finally, the heat loss of the nitrogen coming out from the system is computed with Eq. (4.28).

$$\dot{Q}_{N2,lost} = \dot{m}_{N2} \cdot \overline{c_p}_{N2,Out-U} \cdot (T_{N2,Out} - T_U) \tag{4.28}$$

The heat balance on the window, the absorber and the system is given by the following equations.

$$\dot{Q}_{S,W,rad,a} + \dot{Q}_{A,rad,A-W,a} - \dot{Q}_{W,rad,U} - \dot{Q}_{W,rad,A} - \dot{Q}_{W,conv,U} - \dot{Q}_{W,conv,N2} - \dot{Q}_{W,fcooling} = 0 \tag{4.29}$$

$$\dot{Q}_{S,W,rad,t} - \dot{Q}_{A,rad,A} + \dot{Q}_{A,rad,A-W,r} + \dot{Q}_{A,rad,A-A} + \dot{Q}_{W,rad,A} - \dot{Q}_{A,conv,N2} - \dot{Q}_{I,cond} = 0 \tag{4.30}$$

$$\dot{Q}_{S,W,rad} - \dot{Q}_{S,W,rad,r} - \dot{Q}_{A,rad,A-W,t} - \dot{Q}_{A,rad,A-W,r} - \dot{Q}_{W,rad,U} - \dot{Q}_{N2,lost} - \dot{Q}_{I,cond} - \dot{Q}_{W,conv,U} = 0 \tag{4.31}$$

The program to calculate all these quantities is written with Excel and the iterative tool solver is used to find T_A, T_W, $T_{N2,In}$, $T_{N2,W}$ and $T_{N2,Out}$ to make the heat balance fit. In the target cell, the sum of the square errors of Eqs. (4.29) and (4.30) and of the square errors of estimated $T_{N2,In}$, $T_{N2,W}$ and $T_{N2,Out}$ from the resulted ones from each iterative calculation is set to zero. The system is not linear because the temperatures affect the value of the physical parameters in the equations, but all the functions in the system are derivable: because of this the solver is set to the not linear GRG one, which is the available solver in Excel for such equations system by using the default settings. The system heat balance in Eq. (4.31) is used to check the error of the calculated solutions: for the reference case, the error in the balance is around 0.02 kW, which is the 0.0125% of the net solar power coming to the reactor. For the purpose of this model, this is an acceptable result for the calculations, so no other options have been considered for the solving of the equations.

A reference case has been calculated for the regeneration step because its input power demand is supposed to be higher than for the water splitting step: indeed, the temperature reached on the absorber is 300 °C higher and the mass flow rate of the nitrogen is set to 100 kg/h per reactor, while the one of the water splitting is 10 kg/h per reactor. The input solar power is set to 200 kW, with a 20% of losses due to the losses in the heliostat field and the secondary concentrator: so the net power hitting the window is 160 kW. The heat recovery is fixed at 40%, which ensures a behavior similar to the nitrogen heat exchanger in the plant. The power of the window forced cooling is set to 10 kW. The target is to get a temperature higher than 1400 °C on the absorber and lower than 1000 °C for the quartz window.

The model will be evaluated in the test campaigns in the end of 2016. After that it will be used for finding the best parameters for driving the process.

5. Summary

The EU-funded project Hydrosol Plant concerns the development and implementation of an industrial-scale plant using concentrated solar radiation to split water into its components, hydrogen and oxygen, by a thermochemical cycle with temperatures up to 1400 °C. This paper shows the preliminary design of a solar receiver and the power plant to achieve the cycle. The design concept of the reactor is taken from the SOLREF and REFOS reactors, because it is developed since four generations, ensuring good reliability of the reactor and a good know-how of the institute. However, such high working temperature requires some materials and design changes, which are investigated by DLR in partnership with private companies. About the reactor, another key point would be the metal oxide that will be provided in form of a pure monolith, instead to be coated on a ceramic sublayer: the results of the test campaigns will provide important new data about the two-step thermochemical cycle with nickel-ferrite.

Once the solar reactor will be constructed, some thermal tests will be provided at DLR in Cologne to study its behavior and reliability at high temperature and set some parameters, as the cooling systems. Other tests will be provided directly at the Plataforma Solar de Almería in the end of 2016, when the reactors and the plant should be assembled: these test campaigns will have the main target controlling of the heliostat field and the plant components to reach the operative conditions in the reactors.

With the thermodynamic model it has been calculated that the thermal input power of 750 kW should be enough to reach the

target temperature on all the reactors: indeed, two reactors should operate simultaneously in the regeneration step, so a power around 400 kW should be required. The third reactor should be on the splitting step, which works at 300 °C less than the regeneration one with a flow rate 20 times smaller: for these reasons, the required power is estimated to be lower than for the regeneration step. Thus, the required solar power will be below 600 kW and the rest of the available power will be needed as a reserve for additional losses in all the system which is not taken into account in the model. Because of the slower kinetics in the regeneration step based on the partial pressure of oxygen, which takes more time, each reactor is the double time in regeneration.

The success of the project would mark a major step forward in the technology for the exploitation of solar radiation to produce fuels with thermolysis, since it would be the first time for DLR to operate at such high temperatures with a solar chemical reactor.

Acknowledgements

The work was funded by the Fuel Cells and Hydrogen Joint Undertaking within the Project HYDROSOL-PLANT (GA No. 325361).

References

Abanades, S., Flamant, G., 2006. Thermochemical hydrogen production from a two-step solar-driven water-splitting cycle based on cerium oxides. Sol. Energy 80 (12), 1611–1623.

Agrafiotis, C., et al., 2005. Solar water splitting for hydrogen production with monolithic reactors.

Agrafiotis, C. et al., 2012. Hydrogen production via solar-aided water splitting thermochemical cycles with nickel ferrite: experiments and modeling. Am. Inst. Chem. Eng.

Allendorf, M.D., 2008. Two-step water splitting using mixed-metal ferrites: thermodynamic analysis and characterization of synthesized materials. Energy Fuels 22, 4115–4124.

Allendorf, M.D., et al., 2006. Thermodynamic analysis of mixed-metal ferrites for hydrogen production. In: Proceedings of ISEC2006 ASME International Solar Energy Conference. Denver, Colorado, USA.

Buck, R. et al., 2002. Solar-hybrid gas turbine-based power tower systems (REFOS). J. Sol.Energy Eng. 124, 2.

Ezbiri, M. et al., 2015. Design principles of perovskites for thermochemical oxygen separation. Chemsuschem 8 (11), 1966–1971.

Göhring, F., 2008. Modellierung und Simulation des Betriebsverhaltens eines Receiver–Reaktors zur solaren Wasserstoffproduktion. Diploma Thesis Diploma Thesis. RWTH Aachen.

Gokon, N. et al., 2009. Thermochemical two-step water splitting cycles by monoclinic ZrO_2-supported NiFe_2O_4 and Fe_3O_4 powders and ceramic foam devices. Sol. Energy 83 (4), 527–537.

Han, S.B. et al., 2007. Water splitting for hydrogen production with ferrites. Sol. Energy 81 (5), 623–628.

Houaijia, A. et al., 2013. Analysis and improvement of a high-efficiency solar cavity reactor design for a two-step thermochemical cycle for solar hydrogen production from water. Sol. Energy 97, 26–38.

Kaneko, H., et al., 2006. Two-step water splitting with concentrated solar heat using rotary-type reactor. In: 13th Solar PACES International Symposium, Seville, Spain.

Kodama, T. et al., 2006. A two-step thermochemical water splitting by iron-oxide on stabilized zirconia. J. Sol.Energy Eng. 128 (1), 3–7.

Lemort, F. et al., 2006. Technological and chemical assessment of various thermochemical cycles: from the UT3 cycle up to the two steps iron oxide cycle. Int. J. Hydrogen Energy 31 (14), 2063–2075.

Martin, H., 2006. VDI-Wärmeatlas. Heidelberg, Springer-Verlag, Berlin.

Miller, J.E., 2007. Initial case for splitting carbon dioxide to carbon monoxide and oxygen. Sandia Report SAND2007-8012.

Möller, S., et al., 2006. SOLREF – development of an advanced solar high-temperature reformer. In: Proceedings of ISEC2006: ASME International Solar Energy Conference, Denver, CO, USA.

Morgan®, 2013. Alphawool® Unifelt™ – Data sheet, Morgan Advanced Materials.

Neises, M., 2011. Investigations of mixed iron oxides coated on ceramic honeycomb structures for thermochemical hydrogen production. Ph.D. dissertation. RWTH Aachen.

Opticad-Corporation®, 2008. OptiCAD® – Useŕs Guide – Version 9, Opticad-Corporation®.

Roeb, M. et al., 2006. Thermo-chemical production of hydrogen from water by metal oxides fixed on ceramic substrates. WHEC 16, Lyon France.

Steinfeld, A., 2002. Solar hydrogen production via a two-step water-splitting thermochemical cycle based on Zn/ZnO redox reactions. Int. J. Hydrogen Energy 27 (6), 611–619.

Steinfeld, A. et al., 1999. Design aspects of solar thermochemical engineering – a case study: two-step water-splitting cycle using Fe_3O_4/FeO redox system. Sol. Energy 65 (1), 43–53.

Sturzenegger, M., Nuesch, P., 1999. Efficiency analysis for a manganese-oxide-based thermochemical cycle. Energy 24 (11), 959–970.